Air-clad suspended nanocrystalline diamond ridge waveguides

Abdou, Aly; Panduranga, Parashara; Richter, Jens; Thomas, Evan L. H.; Mandal, Soumen; Williams, Oliver A.; Witzens, Jeremy; Nezhad, Maziar

Optics Express

DOI:
10.1364/OE.26.013883

Published: 15/05/2018

Publisher's PDF, also known as Version of record

Research Article | Vol. 26, No. 11 | 28 May 2018 | OPTICS EXPRESS 13883

Optics EXPRESS

Air-clad suspended nanocrystalline diamond ridge waveguides

ALY ABDOU,[1,4] PARASHARA PANDURANGA,[1,4] JENS RICHTER,[2] EVAN L. H. THOMAS,[3] SOUMEN MANDAL,[3] OLIVER A. WILLIAMS,[3] JEREMY WITZENS,[2] AND MAZIAR P. NEZHAD[1,*]

[1]*School of Electronic Engineering, Bangor University, LL57 1UT, UK*
[2]*Institute of Integrated Photonics, RWTH Aachen University, Sommerfeldstrasse 24, D-52074, Aachen, Germany*
[3]*School of Physics and Astronomy,Cardiff University,Queen's Buildings, The Parade, Cardiff, CF24 3AA, UK*
[4]*These authors contributed equally to the paper*
**maziar@bangor.ac.uk*

Abstract: A hybrid group IV ridge waveguide platform is demonstrated, with potential application across the optical spectrum from ultraviolet to the far infrared wavelengths. The waveguides are fabricated by partial etching of sub-micron ridges in a nanocrystalline diamond thin film grown on top of a silicon wafer. To create vertical confinement, the diamond film is locally undercut by exposing the chip to an isotropic fluorine plasma etch via etch holes surrounding the waveguides, resulting in a mechanically stable suspended air-clad waveguide platform. Optical characterization of the waveguides at 1550 nm yields an average optical loss of 4.67 ± 0.47 dB/mm. Further improvement to the fabrication process is expected to significantly reduce this waveguide loss.

OCIS codes: (130.0130) Integrated optics; (160.6000) Semiconductor materials; (230.7370) Waveguides; (310.0310) Thin films; (350.3850) Materials processing.

References and links

1. Z. G. Hu, P. Prunici, P. Hess, and K. H. Chen, "Optical properties of nanocrystalline diamond films from mid-infrared to ultraviolet using reflectometry and ellipsometry," J. Mater. Sci. Mater. Electron. **18**(S1), 37–41 (2007).
2. B. J. M. Hausmann, B. Shields, Q. Quan, P. Maletinsky, M. McCutcheon, J. T. Choy, T. M. Babinec, A. Kubanek, A. Yacoby, M. D. Lukin, and M. Loncar, "Integrated Diamond Networks for Quantum Nanophotonics," Nano Lett. **12**(3), 1578–1582 (2012).
3. A. H. Piracha, P. Rath, K. Ganesan, S. Kühn, W. H. P. Pernice, and S. Prawer, "Scalable Fabrication of Integrated Nanophotonic Circuits on Arrays of Thin Single Crystal Diamond Membrane Windows," Nano Lett. **16**(5), 3341–3347 (2016).
4. F. Gao, J. V. Erps, Z. Huang, H. Thienpont, R. G. Beausoleil, and N. Vermeulen, "Directional Coupler Based on Single-Crystal Diamond Waveguides," IEEE J. Sel. Top. Quantum Electron. **24**(6), 1–9 (2018).
5. Y. Hirose and Y. Terasawa, "Synthesis of Diamond Thin Films by Thermal CVD Using Organic Compounds," Jpn. J. Appl. Phys. **25**(2), L519–L521 (1986).
6. Y. Liou, A. Inspektor, R. Weimer, and R. Messier, "Low-temperature diamond deposition by microwave plasma-enhanced chemical vapor deposition," Appl. Phys. Lett. **55**(7), 631–633 (1989).
7. O. A. Williams, "Nanocrystalline diamond," Diamond Related Materials **20**(5-6), 621–640 (2011).
8. V. Prajzler, M. Varga, P. Nekvindova, Z. Remes, and A. Kromka, "Design and investigation of properties of nanocrystalline diamond optical planar waveguides," Opt. Express **21**(7), 8417–8425 (2013).
9. N. Gruhler, T. Yoshikawa, P. Rath, G. Lewes-Malandrakis, E. Schmidhammer, C. Nebel, and W. H. P. Pernice, "Diamond on aluminum nitride as a platform for integrated photonic circuits," Phys. Status Solidi., A Appl. Mater. Sci. **213**(8), 2075–2080 (2016).
10. P. Rath, N. Gruhler, S. Khasminskaya, C. Nebel, C. Wild, and W. H. P. Pernice, "Waferscale nanophotonic circuits made from diamond-on-insulator substrates," Opt. Express **21**(9), 11031–11036 (2013).
11. J. S. Penades, A. Ortega-Moñux, M. Nedeljkovic, J. G. Wangüemert-Pérez, R. Halir, A. Z. Khokhar, C. Alonso-Ramos, Z. Qu, I. Molina-Fernández, P. Cheben, and G. Z. Mashanovich, "Suspended silicon mid-infrared waveguide devices with subwavelength grating metamaterial cladding," Opt. Express **24**(20), 22908–22916 (2016).

#326818 https://doi.org/10.1364/OE.26.013883
Journal © 2018 Received 23 Mar 2018; revised 2 May 2018; accepted 3 May 2018; published 15 May 2018
Corrected: 16 May 2018

Optics EXPRESS

12. Z. Cheng, X. Chen, C. Y. Wong, K. Xu, and H. K. Tsang, "Mid-infrared Suspended Membrane Waveguide and Ring Resonator on Silicon-on-Insulator," IEEE Photonics J. **4**(5), 1510–1519 (2012).
13. X. Checoury, D. Néel, P. Boucaud, C. Gesset, H. Girard, S. Saada, and P. Bergonzo, "Nanocrystalline diamond photonics platform with high quality factor photonic crystal cavities," Appl. Phys. Lett. **101**(17), 171115 (2012).
14. D. M. Shyroki, "Exact Equivalent Straight Waveguide Model for Bent and Twisted Waveguides," IEEE Trans. Microw. Theory Tech. **56**(2), 414–419 (2008).
15. E. L. H. Thomas, G. W. Nelson, S. Mandal, J. S. Foord, and O. A. Williams, "Chemical mechanical polishing of thin film diamond," Carbon **68**, 473–479 (2014).
16. M. Malmström, M. Karlsson, P. Forsberg, Y. Cai, F. Nikolajeff, and F. Laurell, "Waveguides in polycrystalline diamond for mid-IR sensing," Opt. Mater. Express **6**(4), 1286–1295 (2016).
17. J. M. Dodson, J. R. Brandon, H. K. Dhillon, I. Friel, S. L. Geoghegan, T. P. Mollart, P. Santini, G. A. Scarsbrook, D. J. Twitchen, A. J. Whitehead, J. J. Wilman, and H. de Wit, "Single crystal and polycrystalline CVD diamond for demanding optical applications," in *Window and Dome Technologies and Materials XII*, Proc. SPIE **8016**, 80160L (2011).
18. F. P. Payne and J. P. R. Lacey, "A theoretical analysis of scattering loss from planar optical waveguides," Opt. Quantum Electron. **26**(10), 977–986 (1994).

1. Introduction

Integrated photonic chip production has developed into a mature technology, with silicon and III-V semiconductor platforms being the dominant materials and the telecommunications spectral window being the main focus of photonic chip research. Expanding this research into other parts of the optical spectrum requires new materials and architectures, mainly due to the absorption bands of the aforesaid materials. In particular, the use of the silicon-on-insulator platform at middle and long infrared wavelengths is limited by the spectral transmission windows of both the buried oxide and silicon device layers in the Silicon-on-Insulator platform.

Diamond is a wide bandgap material with a much larger optical transmission window compared to silicon and III-V materials [1] and is therefore an excellent candidate for photonic chips operating in the UV, visible and infrared spectral regions. Due to its high refractive index (2.39), it allows for the fabrication of sub-micron optical waveguides in integrated photonic chips. Many instances of photonic integrated circuits have been demonstrated using bonded and thinned single crystal diamond layers [2–4]. While the optical quality of the diamond thin films used in this approach is very good, the required bond and layer transfer processes add additional layers of complexity to the fabrication process. In addition, large area single crystals of diamond are expensive and relatively difficult to obtain. As an alternative, polycrystalline diamond thin films can be readily grown on a variety of large area substrates (such as silicon and oxide wafers [5,6]) by chemical vapor deposition (CVD) on a substrate seeded with diamond nanocrystals. Polycrystalline diamond films with nanoscale grain sizes (nanocrystalline diamond (NCD)) inherit a great deal of the optical, mechanical and thermal properties of single crystal diamond and can be used in place of single crystal diamond thin films in numerous applications. Such films can be grown with controlled film stress using a variety of techniques, as reviewed in [7]. Several instances of integrated photonic components have been demonstrated using NCD grown on lower refractive index substrates or buried layers to create vertical confinement [8–10]. While this is perfectly acceptable for operation in the visible and near IR, it prohibits operation at longer wavelengths due to absorption in the lower index cladding. One approach for addressing this issue is to create undercut air-clad suspended waveguides, so that the effect of the cladding is completely removed. While such structures have been demonstrated in several instances using silicon waveguides [11,12], this is not generally the case for diamond and nanocrystalline diamond waveguides, even though suspended diamond waveguides can have a much wider transmission spectrum compared to silicon, thereby increasing the range of possible applications of such integrated photonic chips (e.g., far infra-red gas sensing). One relevant example of a suspended nanocrystalline diamond waveguide is reported in [13], where suspended air-clad rib waveguides guide light into suspended 2-D photonic crystals. The suspended structures are supported by 70 nm nano-tethers to minimize scattering losses from

Optics EXPRESS

the tether points. While this approach offers a novel solution for creating NCD waveguides, the structural dependence on the fragile nano-tethers can compromise mechanical stability and robustness. In addition, due to their small size, patterning the 70 nm nano-tethers cannot be done without electron beam lithography. Finally, the architecture in [13] does not seem to offer a route for electrothermal on-chip tuning, which would be a requirement for creating tunable nanophotonic devices such as ring resonators.

As an alternate route, here we report a hybrid group IV waveguide platform consisting of suspended diamond ridge waveguides fabricated from NCD thin films grown directly on silicon substrates (Fig. 1(a)). This architecture not only creates the necessary vertical and lateral confinement needed to create a confined mode, it also offers a path for complete utilization of the wide optical transmission window of diamond, while being mechanically robust. The support membrane can also be utilized to add metal heatpads for electrothermal tuning. Finally, even though the waveguides here are written using e-beam lithography (for patterning flexibility), this is not an absolute necessity and all the features can be, in principle, patterned using optical lithography. . In the first part of the paper we present the architecture and associated waveguide simulations and design steps. Then we present details of the fabrication process and finally present optical measurements on these suspended waveguides, followed by a discussion on future potential applications of this waveguide platform.

2. Design

Since the NCD layer is grown on silicon substrates, the platform will not inherently possess vertical confinement, due to the considerably larger refractive index of silicon (3.47). While this can be remedied by using a lower index interlayer (such as an oxide layer a few microns thick), we have chosen an alternative route, namely creating a suspended rib waveguide with air cladding above and below it (Fig. 1(a)). As mentioned, this architecture has the advantage of being limited only by the diamond transmission window. In addition, since an appreciable portion of the optical mode lies in the air cladding, it offers a convenient platform for sensing applications, in particular gas sensing. Given this architecture, all the optical simulations have been carried out for a suspended air-clad ridge waveguide, under the assumption that the void is large enough to optically isolate the diamond layer from the silicon substrate. The 1550 nm telecommunications wavelength was chosen for the design, due to the technological relevance of this wavelength and availability of test equipment, however the same approach can be easily adapted to longer wavelengths.

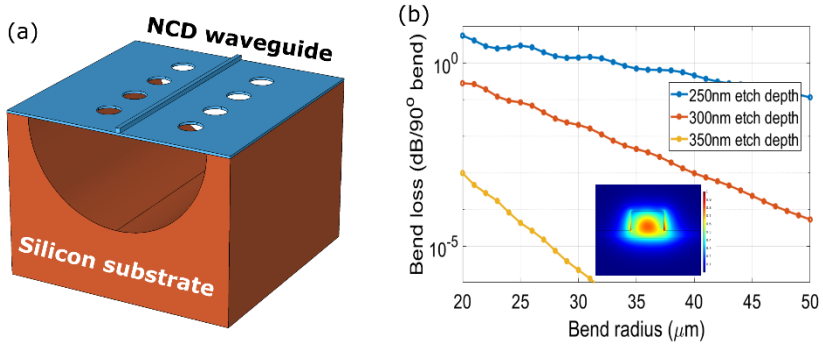

Fig. 1. (a) Schematic of the proposed structure. (b) Loss vs bend radius for various etch depths.

The test wafer consisted of a polished 520 nm NCD layer grown on silicon, on which partially etched waveguide ridges were created. The major constraint in designing the waveguide structure is the ridge etch depth. A shallow etch will result in a weakly confined optical mode, which will limit the bend radius. On the other hand, a deep etch will result in a very thin support membrane, thereby compromising the structural integrity of the device.

Optics EXPRESS

Figure 1(b) depicts the bend losses at 1550 nm vs. etch depth for a 600 nm wide ridge waveguide, etched from a 520 nm diamond membrane. Bend losses were calculated using a finite element solver (COMSOL) and an exact mapping of Cartesian to curvilinear coordinates [14]. From this, we deduced that an etch depth of 350 nm, corresponding to a 170 nm support membrane will provide a good compromise between optical confinement and mechanical integrity, while ensuring single mode quasi-TE operation. The quasi-TE mode distribution is depicted in the inset of Fig. 1(b).

Inverse taper edge-couplers were designed for coupling light in and out of the waveguides. The edge-coupler was chosen due to the broadband nature of the coupling and fabrication simplicity. Assuming a single etch depth throughout the chip, the coupling efficiency between a flat single mode fiber facet and the taper was simulated, resulting in a calculated optimized coupling of 83% for a 300 nm wide inverse taper coupler.

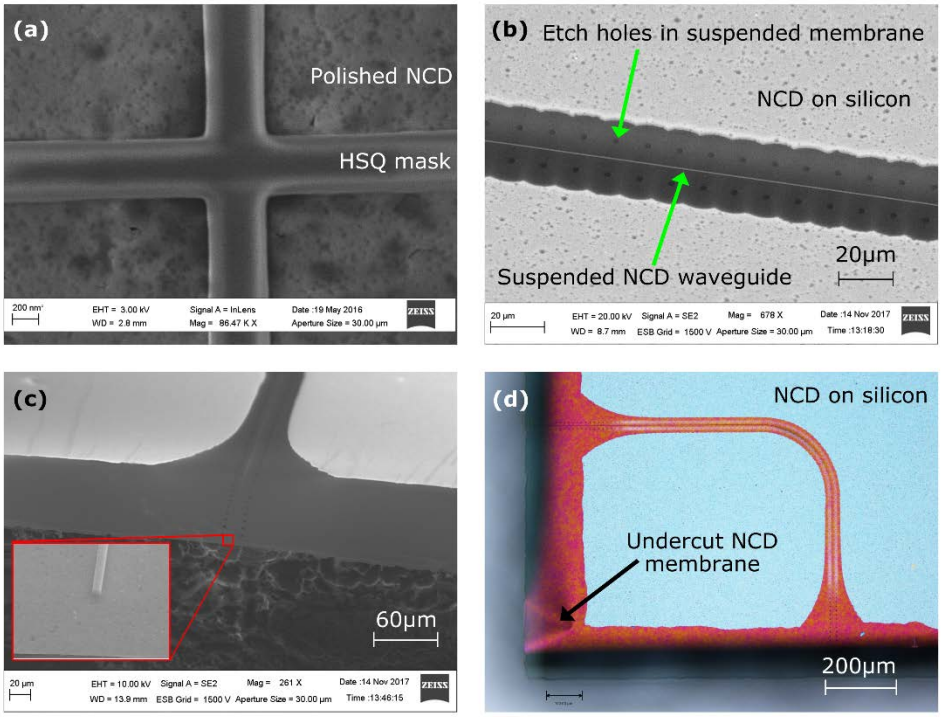

Fig. 2. (a) SEM image of NCD surface after e-beam lithography of HSQ etch mask, (b) SEM image of the undercut waveguide and membrane, (c) SEM image of the input waveguide taper showing membrane sag (d) optical image of an undercut waveguide showing the sagging edges on the chip.

3. Fabrication

The NCD was grown on a 500 μm thick, highly doped silicon wafer, as reported in [15].First, a mono-dispersed nanodiamond solution was applied in an ultra-sonic bath for 10 minutes to seed the silicon wafer. A 600 nm thick layer of diamond was grown on top of the silicon surface through CVD (CH_4 at 5 sccm; H_2 at 475 sccm; Pressure = 40 Torr; Power = 3500 W Time: 298 minutes; Temperature = 842° C). The film was grown with an initial 5 min incubation period of 25 sccm CH_4 to establish the seeds before reducing to 5 sccm for the remainder of growth. The film was then thinned down to 520 nm through chemical mechanical polishing (using colloidal silica fluid, Logitech SF1) to achieve an RMS surface roughness value below 2 nm. An array of L-shaped suspended diamond ridge waveguides of lengths ranging from 1.524 to 4.524 mm was chosen for the study. The waveguides were

Optics EXPRESS

fabricated via electron beam lithography, optical lithography and dry etching steps. First, the ridge was patterned using hydrogen silsesquioxane (HSQ) using electron beam lithography (Vistec EBPG5200, 100 kV) (Fig. 2(a)). The diamond film was then etched anisotropically down to 170 nm in order to form the ridge waveguide using reactive ion etching (RIE) with O_2 at 30 sccm, pressure = 65 mTorr and RF power = 100 W. This recipe provided the desired vertical side walls and had an etch rate of about 60 nm/minute. The HSQ mask was removed using a hydrofluoric acid dip and a 40 nm thick chromium mask was then deposited on top of the partially etched diamond film. Optical lithography and a chromium wet etch (CR-7) were used to pattern the etch holes (3.3 μm diameter each) in the chromium mask. This pattern was transferred to the diamond film through a second anisotropic etching step using the same oxygen RIE parameters, after which the entire chromium film was removed using CR-7.

All wet processing steps were performed before undercutting the diamond film, to reduce the chances of damaging the undercut structures. Finally, the silicon substrate was isotropically dry etched through the diamond holes using a pure SF_6 ICP-RIE etch step (50 sccm SF_6, 30 mTorr, 1500 W ICP power, 0 RF power). While the etch rate of the isotropic silicon undercut step is quite high (approximately 4 μm/min for an unpatterned silicon surface), this was considerably reduced due to the limiting effect of the small holes in the diamond film. As a result, a 60 minute etch step was required for complete removal of the silicon from beneath the waveguide ridge (Fig. 2(b)), resulting in a 20 μm radius half-cylinder trench (measurement based on the optical image in Fig. 2(d)). Note that the trenches flare out at the start and end of the waveguides, due to the larger etch rate at these locations. Thin film thickness measurements on the diamond film revealed that it had been etched down at a rate of 1nm/min in the SF_6 ICP plasma. As a result, the diamond support membrane and the top of the ridge had also been etched down 60nm in the process of isotropic silicon removal. The lateral dimensions of the waveguides were not affected, which suggests a vertical physical etch component to the nominally isotropic SF_6 etch. While this phenomenon did not substantially affect the waveguide mode, it is still preferable to avoid or minimize it if possible, since it contributed to increased surface roughness on the top of the diamond waveguide ridge. This can be achieved by using larger etch holes (to shorten the overall undercut time) or by using a non-plasma isotropic silicon etch process such as XeF_2 to avoid any unintended reactive ion acceleration due to residual charges. Another side effect of the lengthy isotropic etch step was to create a larger than intended undercut on the edge of the chips, where the input and output tapers were situated. This is due to the fact that the etch rate of the unmasked silicon on the chip edges is much faster compared to etching through the holes in the diamond film. Due to this and the thinning of the support NCD membrane (in the SF_6 etch step), the edges of the diamond membrane exhibited a noticeable sag (Figs. 2(c) and 2(d)) which was different across the waveguides, depending on the position of the waveguides on the chip. This causes a drop in the edge coupling efficiency and is a motivating factor for moving towards other light coupling mechanisms such as grating coupling, since a grating coupler fabricated on a suspended membrane would be supported on all sides, thus drastically reducing the membrane sag.

4. Optical measurements

Polarized light from a tunable telecommunications laser was injected into the L-shaped waveguides using a lensed fiber. The original objective was to use the cutback method for loss measurements but the unexpected non-constant coupling between waveguides due to the varying membrane sag and the large amount of scatter from the waveguides prompted us to instead use the scattered light for quantifying the waveguide losses. The scattered light was collected using a near-infrared camera (Xenics Xeva 640) viewing the chip from the top (Fig. 3(a)). The obtained images were then processed to extract the optical losses by calculating the power drop along a horizontal or vertical segments of four different waveguides, under the assumption of uniform roughness scattering, and then fitting the results to an exponentially

Optics EXPRESS

decaying function $P(L) = P(0)e^{-\alpha L}$, where $P(L)$ is the relative scattered power at the end of the segment and $P(0)$ is the relative power at the beginning of the segment (Fig. 3(b)). The bend sections were not included in the calculations. Scattered power at each point along the waveguide was estimated by integration across the waveguide width. An average loss coefficient of 4.67 ± 0.47 dB/mm has been extracted from the measurements listed in Table 1 with good fit (R^2 value above 0.9). It is of interest to note that while these loss numbers are higher than reported values for single crystal diamond waveguides, they are in the vicinity or smaller than other reported NCD waveguides [10,13,16]. This is likely due to the improved overall qualities of our NCD films that were grown and polished using the techniques outlined in [15]. For comparison, even though the surface roughness of the diamond film used in [13] is reported to be much lower than our etched final waveguide roughness (1.6 nm vs 27 nm), their losses are in the same range (5 – 7 dB/mm). This may be due to the larger granularity in their diamond film (based on the SEM view of the diamond film.)

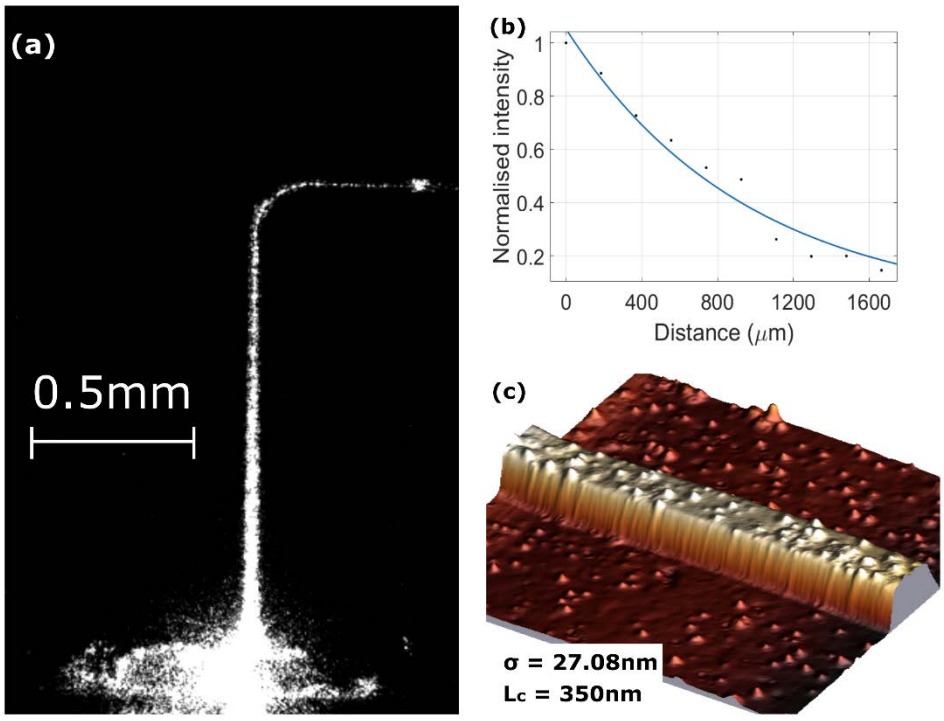

Fig. 3. (a) IR image of the scattered light at 1.55 μm, (b) Example of power decay measurement fitting (R^2 = 0.96), (c) AFM image of waveguide ridge with roughness measurements.

Since the losses of optical grade single-crystal and polycrystalline diamond [17] are much smaller than the values obtained through the loss measurement, other loss mechanisms need to be considered. The SEM image of the surface of the diamond film before etching (Fig. 2(a)) shows some dark spots that may indicate foreign particles in the diamond film, possibly from the silica-based polishing fluid. AFM imaging of the final waveguides shows a large amount of roughness on the top surface, as indicated in Fig. 3(c).The presence of the silica polishing material in conjunction with the SF_6 etch step may be a contributor to this roughness (acting as nanoscale mask points) and it is likely that this roughness is the main source of optical losses in the NCD waveguides. This is supported by the considerable amount of scattered light in the IR images. It should be noted that none of these issues are

Optics EXPRESS

inherent to NCD films and they can be addressed with appropriate adjustments to the growth and polishing steps.

Table 1. Average loss measurements of various waveguides' segments.

#	*L* (μm)	*P(L)/P(0)*	R^2	*Loss* (dB/mm)
1	600	0.35	0.96	8.35
2	1000	0.52	0.92	3.41
3	1000	0.53	0.92	3.12
4	1050	0.53	0.93	3.50
5	1134	0.26	0.96	5.36
6	1150	0.31	0.94	3.93
7	1668	0.17	0.95	5.03

To analyse the effect and contribution of the roughness on the waveguide performance, we attempted to estimate the predicted losses using a scattering model. The total waveguide propagation loss is given as $\alpha = \alpha_{bulk} + \alpha_{rs}$ where α_{rs} is the scattering due to rough waveguide surfaces and other effects. Since the NCD film is grown on a polished silicon surface and the roughness of the sidewall is much smaller than the top, only the roughness on the top surface was considered. Some additional loss due to scattering from voids between the nanocrystalline grains may be present, however for a first order estimate this again was considered negligible compared to the large waveguide surface roughness. The absorption coefficient of bulk diamond at 1.55 μm is approximately 0.01 db/mm [17]. α_{rs} was estimated using the roughness scattering formula for the TE_0 slab mode, developed by Payne and Lacey [18]. The model relates the optical scattering loss from rough surfaces to the RMS roughness σ according to the equations:

$$\alpha_{rs} = \frac{\sigma^2}{\sqrt{2}k_0 d^4 n_1}\cdot g \cdot f(x,\gamma), \qquad g = \frac{U^2V^2}{1+W}$$

$$f(\chi,\gamma) = \chi\sqrt{\frac{\sqrt{(1+\chi^2)^2+2\chi^2\gamma^2}+1-\chi^2}{\sqrt{(1+\chi^2)^2+2\chi^2\gamma^2}}}, \quad \chi = W\frac{L_c}{d}, \quad \gamma = \sqrt{\frac{2n_2^2}{n_e^2-n_2^2}} \qquad (1)$$

$$U^2 = k_0^2 d^2 (n_1^2 - n_e^2),\ V^2 = k_0^2 d^2 (n_1^2 - n_2^2),\ W^2 = k_0^2 d^2 (n_e^2 - n_2^2)$$

where n_1, n_2 and n_e are the core, cladding and effective indices, k_0 is the free space wave number, d is half the slab thickness and L_c is the roughness correlation length. $f(\chi,\gamma)$ is the roughness spectral density function and g accounts for the effect of the waveguide structure and refractive indices. From the AFM measurement, the top surface σ and L_c are estimated to be 27 nm and 350 nm. These were calculated from the standard deviation and Fourier spectrum of the roughness scans, respectively. Using these parameters, the estimated waveguide loss is 4.7 dB/mm, which is reasonably close to the measured values. Additional scattering from sidewall roughness and occasional defects, contamination and voids in the film may appreciably increase this value (e.g., for waveguide #1 in Fig. 3(d)). Based on this analysis, it is reasonable to expect that improvements in the fabrication process which target the roughness of the top waveguide surface will result in a marked improvement of the waveguide loss characteristics. In particular, using the roughness parameters of the original unprocessed film (σ = 2 nm and L_c = 60 nm), the predicted scattering loss is 0.11 dB/mm, which will be a drastic improvement in loss performance. Potential improvements can be effected by using a chemical gas etch step (such as XeF_2) for undercutting the silicon layer, increasing the size of the etch holes and by allowing the e-beam resist to remain on the top of the waveguide ridge until after the undercut is finished. The result of these improvements are planned to be reported in future publications.

In conclusion, we have demonstrated a hybrid silicon/diamond suspended air-clad waveguide platform fabricated from nanocrystalline diamond thin films for operation at 1550 nm. Due to the wide transmission window of diamond, this platform can be easily scaled to

Optics EXPRESS

operate over a wide section of the optical spectrum, covering the UV to the far infrared and therefore can have a large range of applications ranging from visible light integrated photonics to far-infrared optical sensing.

Funding

Welsh Government Sêr Cymru National Research Network in Advanced Engineering and Materials (NRN 105).

Acknowledgements

The authors would like to acknowledge the cleanroom staff at Leeds University (LENNF), Manchester University (National Graphene Institute) and the University of California San Diego (NANO3) for their assistance with various aspects of fabricating the devices described in this article. We also acknowledge the financial support provided by the Welsh Government and Higher Education Funding Council for Wales through the Sêr Cymru National Research Network in Advanced Engineering and Materials (NRN 105).